Engineering Journal issn: 0125-8281

Article

Coastal Upwelling Investigation in the Gulf of Thailand Using Ekman Transport and Sea Surface Temperature Upwelling Indices

Pacharamon Sripoonpan[1,a] **and Suriyan Saramul**[1,2,b,*]

1 Department of Marine Science, Faculty of Science, Chulalongkorn University, Bangkok 10330, Thailand
2 Marine Ecology and Utilization of Marine Resource Research Unit, Aquatic Resources Research Institute, Chulalongkorn University, Bangkok 10330, Thailand
E-mail: [a]pacharamon_sri@outlook.com, [b,*]Suriyan.S@Chula.ac.th (Corresponding author)

Abstract. Two different upwelling indices: (1) Ekman transport upwelling index (UI_{ET}) and (2) sea surface temperature upwelling index (UI_{SST}) were evaluated to determine likely locations of coastal upwelling occurring in the Gulf of Thailand (GoT). GoT covers the area between longitude 98.0°E to 106.0°E and latitude 5.0°N to 14.0°N. In addition, inter-annual and annual variability of UI_{ET} along the east and west coasts were also investigated. UI_{ET} was estimated using monthly averaged wind velocity during 2003–2018, while UI_{SST} was calculated based on the difference between coastal and oceanic monthly mean sea surface temperature at the same latitude. Based on spatial UI_{ET}, favorable upwelling conditions existed mainly along the east and west coasts during northeast and southwest monsoons, respectively. Furthermore, the favorable upwelling conditions were also found sparsely along the east coast and the west coast during the first and second inter-monsoon. The spatial UI_{SST} showed favorable upwelling condition along the west and east coasts around Ca Mau Cape during northeast and southwest monsoons. Meanwhile, during first and second inter-monsoons, the favorable upwelling conditions rarely occurred. Disagreement of spatiotemporal coastal upwelling between UI_{ET} and UI_{SST} were likely due to the shallowness and bottom friction in the GoT. Considering inter-annual variability of meridionally averaged UI_{ET} along east and west coasts, it was found that favorable/unfavorable upwelling conditions were associated with Multivariate ENSO Index signal. Interestingly, annual cycle of meridionally averaged UI_{ET} along west and east coasts showed alternation of favorable and unfavorable upwelling conditions.

Keywords: Upwelling index, monsoon wind, spatiotemporal, MUR-SST, ECMWF.

ENGINEERING JOURNAL Volume 25 Issue 7
Received 1 July 2020
Accepted 27 July 2021
Published 31 July 2021
Online at https://engj.org/
DOI:10.4186/ej.2021.25.7.1

DOI:10.4186/ej.2021.25.7.1

1. Introduction

Coastal upwelling is the upward movement of dense, cool, and nutrient-rich water from the bottom which in turns displaces the surface water; this usually occurs along ocean coastlines [1, 2]. The upwelled, nutrient-replete water can support the growth of phytoplankton which serves as the base of the marine food web. This upwelled water can sustain high primary productivity and high fisheries catch [3, 4, 5]. Several mechanisms are used to explain coastal upwelling such as Ekman pumping induction, dynamic uplift, tidal-induced upwelling, coastal trapped wave, and classical wind-driven flow theory which attributes the coastal upwelling to winds. Wind-driven coastal upwelling is mainly influenced by alongshore winds. In the northern hemisphere, the winds blowing to the right of coastline can generate Ekman transport perpendicular to shoreline which causes the divergence of surface water. Therefore, the water underneath moves upward to replace surface water moving offshore [6, 7, 8]. This similar phenomenon occurs in opposite for the southern hemisphere, since Coriolis force is one of the main forcings in wind-driven upwelling dynamics.

The coastal upwelling index (UI_{ET}) is commonly estimated by using the wind-driven Ekman transport (volume). It is used to indicate the amount of surface water driven offshore and replaced by upwelled water. However, the UI_{ET} refers to only the possible effect of wind on ocean and does not represent any real oceanic variables. Furthermore, the sea surface temperature (SST) difference between coastal and oceanic waters over the same latitude can be also used to identify the coastal upwelling. This so-called the SST upwelling index (UI_{SST}), is also used as an indicator of coastal upwelling. The weakness of using UI_{SST} to predict upwelling is that the gradient of SST does not directly attribute to coastal upwelling because the external factors like river discharge input and air-sea interactions, easily effect on SST [9, 10, 11].

The Gulf of Thailand (GoT), covering area roughly between longitude 98.0°E to 106.0°E and latitude 5.0°N to 14.0°N, is located on the southwestern part of South China Sea (SCS) continental shelf or Sunda Shelf. The area of the GoT is approximately 35,000 km^2 and it is largely enclosed by the land masses of Malaysia, Thailand, Cambodia, and Vietnam (see Fig. 1). The GoT is meridionally divided into 3 parts, Upper Gulf (12.5°N to 13.5°N), Central Gulf (9.0°N to 12.5°N), and Upper Gulf (6.0°N to 9.0°N). Northeast monsoon and southwest monsoon mainly control climate and seasonal variations of water circulation in the GoT. Northeast monsoon typically lasts from November to February, while southwest monsoon lasts from May to September. In between northeast and southwest monsoons, there are two inter-monsoons. The first inter-monsoon lasts from March to April and second inter-monsoon is in October. The GoT is also an important fishery resource providing a huge income to the country through the fishery industries, tourisms, and port operations [12, 13].

Several observations on coastal upwelling in the GoT point to the occurrences along the east coast during northeast monsoon and along the west coast during southwest monsoon [14, 15, 16]. This coastal upwelling is also related to the counterclockwise circulation along the west coast during southwest monsoon [17]. Additionally, the circulation features in the GoT were investigated by applying ocean color data to representing the chlorophyll_a concentration often used as an indicator of phytoplankton biomass and one of possible signs of upwelling condition [18]. As the result of [18]'s study, the high chlorophyll_a concentration was found year round around Samui Island, Surat Thani province (see Fig. 1 for location of Samui Island). Samui Island is Thailand's third largest island located at 100°E and 10°N with an area of 247 km^2 [19]. Samui Island is also an important tourist destination due to its high marine biodiversity and beautiful sandy beaches [20]. Furthermore, water near Sumui Island is also believed to be one of spawning grounds of short mackerel found in the GoT.

To effectively manage the living resources management and handle fishery-related problems in the GoT, we need to have the in-depth understanding in coastal upwelling which might provide geographical mapping and mechanism of fisheries resources (e.g., habitats, fish eggs, nursery, and larvae grounds) [21, 22, 23, 24]. Since, the comprehensive knowledge of coastal upwelling in the GoT is still lacking, this study focuses on the seasonal variability of coastal upwelling found in the GoT as investigated through the upwelling index estimation using two different approaches, Ekman transport and gradient of sea surface temperature between coastal and oceanic waters.

2. Methodology

To describe seasonal coastal upwelling found in the GoT, two different upwelling indices which are Ekman transport upwelling index and sea surface temperature index are evaluated in this study. Details of each approach and how to calculate them are described below.

2.1. Ekman Transport Upwelling Index (UI_{ET}) Estimation

The 10-m monthly mean of daily mean zonal and meridional wind components during 2003–2018 with resolution of $0.125° \times 0.125°$ were downloaded from the European Centre Medium-range Weather Forecast, in short ECMWF (https://www.ecmwf.int/). This data is so-called ECMWF Reanalysis Interim or ERA-Interim [25]. It is the global atmospheric reanalysis data set covering from the period of 1979 to present, and offering online and near-real time data of various atmospheric parameters.

To visualize the upwelling characteristics in the GoT, monthly mean wind components mentioned above were used to calculate Ekman transport upwelling index through the following equations (Eqs. (1)–(5)) as described by [11],

$$Q_x = \frac{\tau_y}{\rho_w f} \tag{1}$$

$$Q_y = \frac{\tau_x}{\rho_w f} \tag{2}$$

$$\tau_x = \rho_a C_D W_{10x} \sqrt{W_{10x}^2 + W_{10y}^2} \tag{3}$$

$$\tau_y = \rho_a C_D W_{10y} \sqrt{W_{10x}^2 + W_{10y}^2} \tag{4}$$

$$UI_{ET} = -\left[\sin\left(\varphi - \frac{\pi}{2}\right) Q_y + \cos\left(\varphi - \frac{\pi}{2}\right) Q_x\right] \tag{5}$$

The east-west and north-south Ekman transport (Q_x and Q_y) are expressed in Eqs. (1) and (2), respectively, where τ_x is zonal wind stress, τ_y is meridional wind stress, $\rho_w = 1025$ kg/m^3 is the density of seawater, and $f = 2\Omega \sin\theta$ is the Coriolis parameter ($\Omega = 7.292 \times 10^{-5}$ rad/s is the Earth's angular velocity and θ is latitude laid between 6°N and 14°N). The zonal and meridional wind stresses are determined using empirical formula as presented in Eqs. (3) and (4), respectively, where $\rho_a = 1.22$ kg/m^3 is air density, $C_D = 1.3 \times 10^{-3}$ is a constant dimensionless drag coefficient, W_{10x} and W_{10y} are wind speed at 10 m above mean sea level in east-west and north-south directions, respectively [9]. Generally, the Ekman transport is the magnitude of two transport vectors which are the east-west and north-south transport (Q_x and Q_y). Finally, the Ekman transport upwelling index, UI_{ET}, is defined in Eq. (5), where φ is an angle between coastline and equator. For instance the western side of the Upper Gulf (see Fig.1) has $\varphi = -90°$, while the eastern side has $\varphi = 90°$. A positive value of UI_{ET} means a favorable upwelling condition, while a negative value of UI_{ET} means an unfavorable upwelling condition [11, 26, 27]. Hence, negative and positive values of UI_{ET} will be

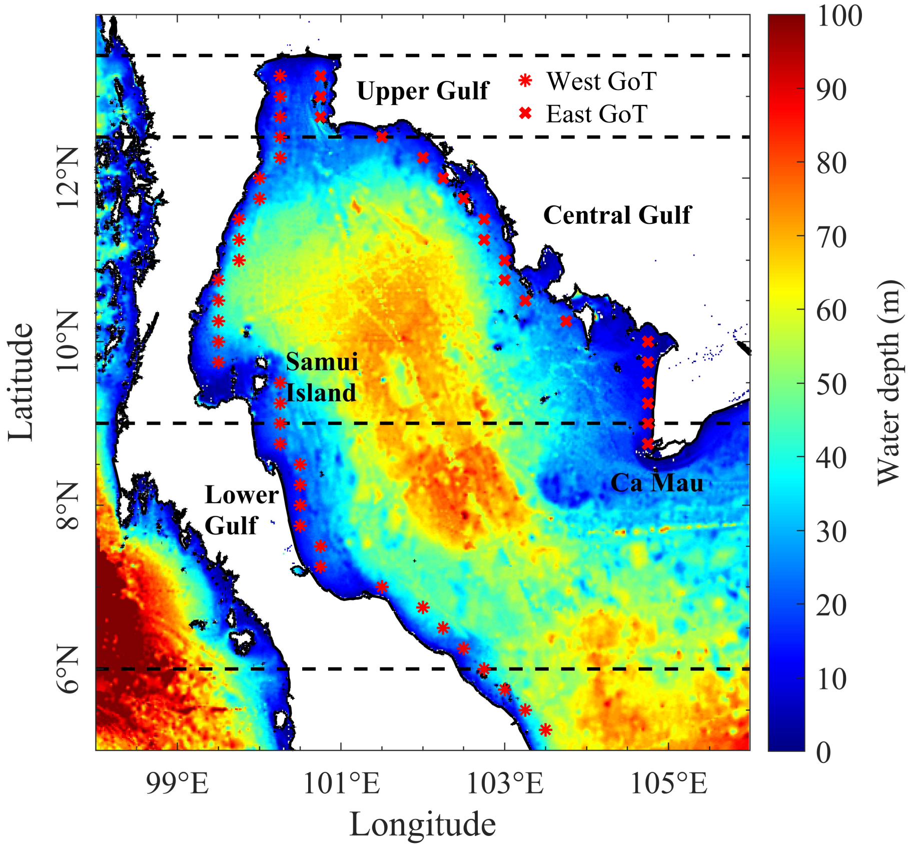

Fig. 1. Study area (the Gulf of Thailand). The Upper Gulf, Central Gulf, and Lower Gulf are defined and separated by black dash line. Red asterisks and red crosses are locations, where spatio-temporal of Ekman Transport Upwelling Index were analyzed.

used to separate upwelling area/occurrence from downwelling area/occurrence.

2.2. Sea Surface Temperature Index (UI_{SST}) Estimation

The satellite-derived cooling of surface water displaced by the upwelled water is another potential proxy of the coastal upwelling detection [28, 29]. The global daily multi-scale ultra-high resolution sea surface temperature analysis (MUR-SST; see more detail in [30, 31]), which is longest and finest observation of SST recorded by satellite instruments during 2003–2018 were retrieved from the Physical Oceanography Distributed Active Archive Center or PODAAC's website (https://podaac.jpl.nasa.gov/). This data set was spatially averaged to obtain monthly averaged SST. To reveal the upwelling characteristics found in GoT, the upwelling index based SST (UI_{SST}) was then estimated using Eq. (6) [11, 32]. Equation (6) defines the gradient of SST between coastal SST ($SST_{coastal}$; it is either the nearest to shoreline of narrow continental shelf or slightly separated from the shoreline) and the oceanic SST ($SST_{oceanic}$; it is offshore temperature with a distance of 2 degree along the same latitude). It should be noted that the SST accuracy is particularly dependent on its spatial resolution [33]. The negative value of UI_{SST} means favorable upwelling condition, while a positive UI_{SST} means unfavorable upwelling condition [9, 26, 27].

$$UI_{SST} = SST_{coastal} - SST_{oceanic} \tag{6}$$

3. Results and Discussions

3.1. Seasonal Wind Patterns

Seasonal wind patterns in GoT are shown in Fig. 2. These patterns were based on 16-year long monthly averaged wind vector. In January, which represents northeast monsoon (see Fig. 2(a)), northeasterly wind dominated in the Upper Gulf and the entrance of the GoT, while easterly wind is mostly found in the Central Gulf. Generally, the strong wind speeds (4–5 m/s) were observed at the Lower Gulf and their speeds gradually decreased toward the Upper Gulf (1–2 m/s). This pattern was also found during the first inter-monsoon (March), where the wind field seemed to blow westward in the Lower Gulf, northwestward in the Central Gulf, and northward in the Upper Gulf (see Fig. 2(b)). However, the magnitudes of wind vectors were quite similar (about 4–5 m/s) for the whole GoT.

Figure 2(c) depicted wind pattern in August, which represents southwest monsoon. In this period, winds mainly prevailed east-northeastward in the Central Gulf. In the Upper Gulf and Lower Gulf, southwesterly winds were the major influences. Apart from wind direction, wind speeds of 4–5 m/s were found almost for the whole Gulf. During the second inter-monsoon (October), weak winds (1–2 m/s) blew southward to southeastward in the Upper Gulf and Central Gulf, respectively (see Fig. 2(d)). From Fig. 2, the impact of East Asian and Indian monsoons on wind patterns in the GoT can be noticed. Wind patterns at the Upper Gulf and Lower Gulf clearly prevailed in northeast and southwest direction depending on monsoon winds. However, in the Central Gulf wind patterns were mainly easterly and westerly during northeast and southwest monsoons, respectively. These monsoonal wind patterns shown in Fig. 2 will be used to estimate the upwelling index in the following section.

3.2. Ekman Transport and UI_{ET}

Using Eqs. (1)–(4), the magnitude and direction of Ekman transports can be calculated using seasonal wind velocity components as previously analyzed in section 3.1 (see Fig. 3). Theoretically, the Ekman transports obviously move perpendicular to wind vector. In northern hemisphere, it is to the right of wind direction and vice versa in southern hemisphere. The stronger the wind speed, the more transported water. Hence, during northeast monsoon (January; Fig. 3(a)) strong transport from SCS moved northwestward into the Lower Gulf and turned north toward Central Gulf. While weak northwestward transport appeared in both the Upper Gulf and Central Gulf. In addition, SCS's water that moved into the Gulf mostly propagated from the west coast of Vietnam during northeast monsoon [34]. Based on wind speed shown in Fig. 2(a), strong and weak transport were found in the Lower Gulf and Upper Gulf, respectively.

For the first inter-monsoon (see Fig. 3(b)), the strongest transport still existed in the Lower Gulf, while weak transport occurred in the Central and Upper Gulfs. The transport directions moved into the GoT from the Lower Gulf and turned northeastward and eastward at the Central Gulf and Upper Gulf, respectively. These patterns were related to the directions of wind as depicted in Fig. 2(b). The movements found during this period can cause the water to pile up in the eastern GoT. During the southwest monsoon (see Fig. 3(c)), the strong north-northeastward wind appeared for the whole Gulf causing water be transported out of the GoT. Unlike other monsoons, the second inter-monsoon's transport was very minimal (see Fig. 3(d)). Note that vector scale in Fig. 3(d) is different from others with 5 orders of magnitude smaller. However, transport found in this period was eventually opposite to the

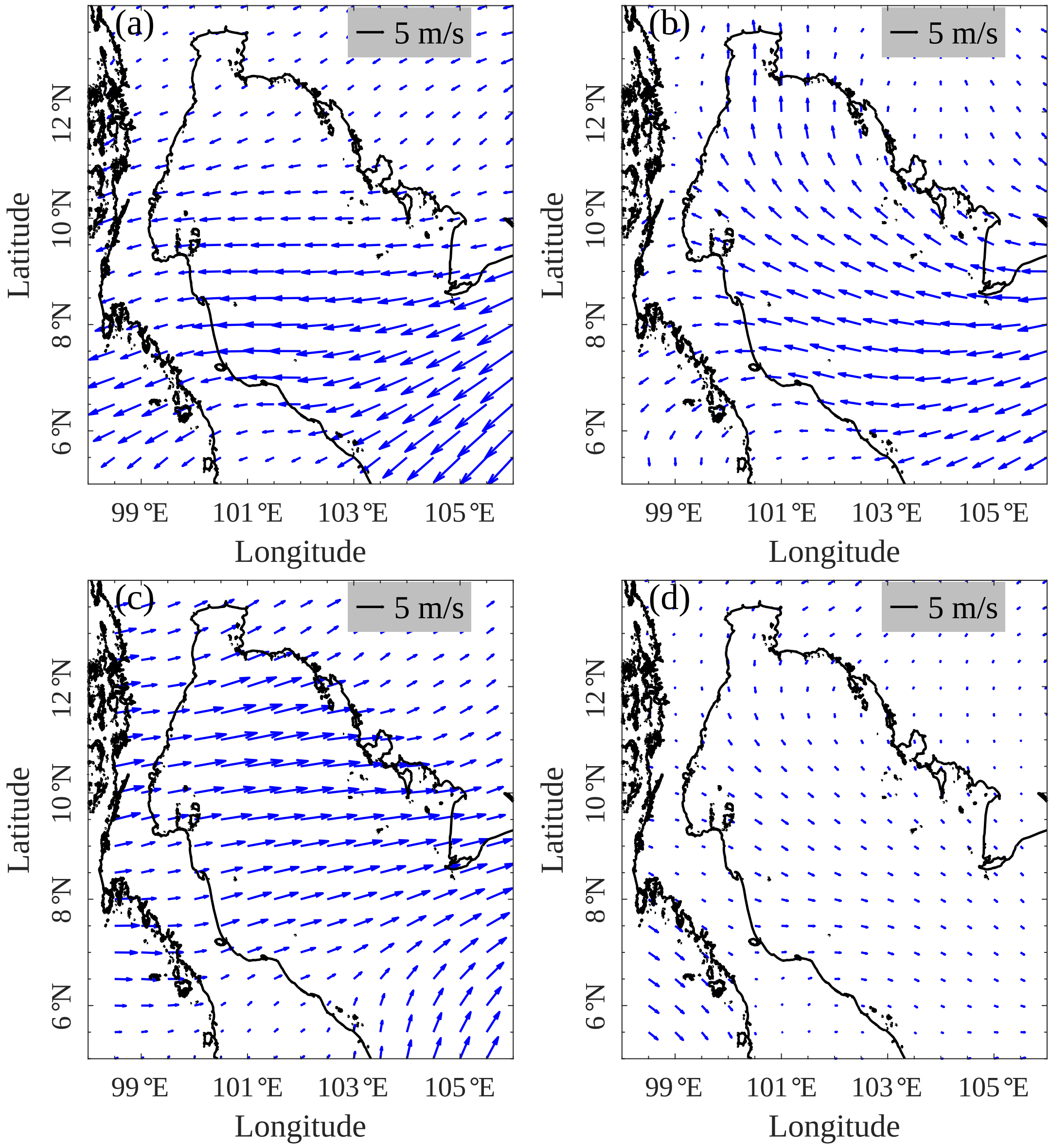

Fig. 2. Surface wind vector (m/s) in (a) January (Northeast monsoon), (b) March (1st inter-monsoon), (c) August (Southwest monsoon) and (d) October (2nd inter-monsoon).

transport of first inter-monsoon. This means that transport for the whole Gulf tended to move toward the western GoT (the piling up of water was found in the western GoT).

From Fig. 3, conclusion can be drawn that Ekman transport pushed water in and out GoT during northeast and southwest monsoons, respectively. As a result, higher and lower seasonal sea levels were found in the GoT during northeast monsoon, November–February, and during southwest monsoon, May-September (see Fig. 8(a)–(d) in [35]), respectively. In addition, during northeast and southwest monsoons the Ekman transport near Samui Island (for location see Fig. 1) seemed to agree to surface current shown in [36]. The surface currents near Samui Island moved northwestward during northeast monsoon and eastward during southwest monsoon. For the first and second inter-monsoon, water in the GoT had been pushed toward the eastern and western GoT, respectively.

To investigate upwelling/downwelling areas in GoT, Ekman transport upwelling index (UI_{ET}) was determined by considering the transport directions, shown in Fig. 3, to the shoreline angle with respect to the Equator. Generally, the offshore transport will be considered as upwelling favorable and vice versa for the shoreward transport. Figure 4 demonstrates the upwelling condition based on Ekman transport upwelling index for 4 different monsoons. As mentioned above, the direction of Ekman transport during northeast and southwest monsoons were in opposite directions, hence upwelling and downwelling areas were also presented in opposite location depending on what monsoon is taken

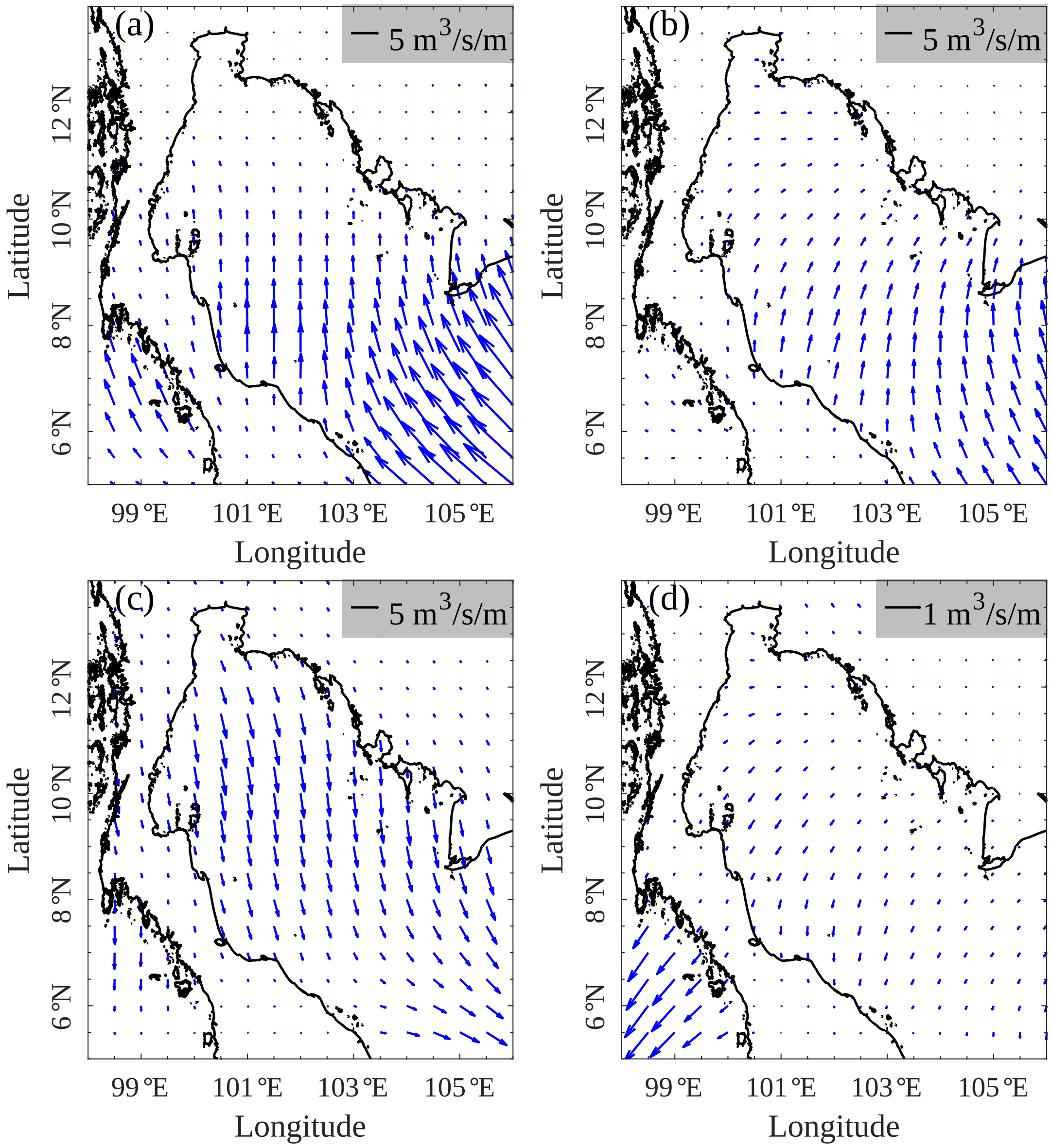

Fig. 3. Ekman transport ($m^3/s/m$) in (a) January (Northeast monsoon), (b) March (1st inter-monsoon), (c) August (Southwest monsoon) and d) October (2nd inter-monsoon). Blue arrows denote Ekman transport (magnitude and direction). Remark: black arrow scale shown in (d) is about 5 times smaller than others.

into consideration. This is also true for the first and second inter-monsoon. In general, favorable upwelling condition existed along the west coast of the GoT during northeast monsoon and first inter-monsoon, except some areas, such as the western side of the Upper Gulf down to the western side of the Central Gulf (see Fig. 4(a) and 4(b)).

Conversely, along the eastern side of the GoT, favorable upwelling conditions were found along the east coast of the Upper Gulf during northeast monsoon and along the western side of Ca Mau Cape during the first inter-monsoon. During southwest and second inter-monsoon, favorable upwelling condition generally occurred along the east coast of the GoT, except the west coast of the Upper Gulf during southwest monsoon and the western side of Ca Mau Cape during the second inter-monsoon (see Fig. 4(c) and 4(d)). Furthermore, favorable upwelling conditions also found along the western side of the Upper Gulf down to the Lower Gulf during southwest monsoon. The locations of favorable upwelling conditions obtained in this section were based upon the Ekman transport caused by wind phenomena (more detail analysis will be discussed in section 3.5). It is worth noting that not only Ekman transport used to identify upwelling area, but also other parameters, such as sea surface temperature gradient between near-shore and offshore. This upwelling index based SST will be demonstrated in the following section.

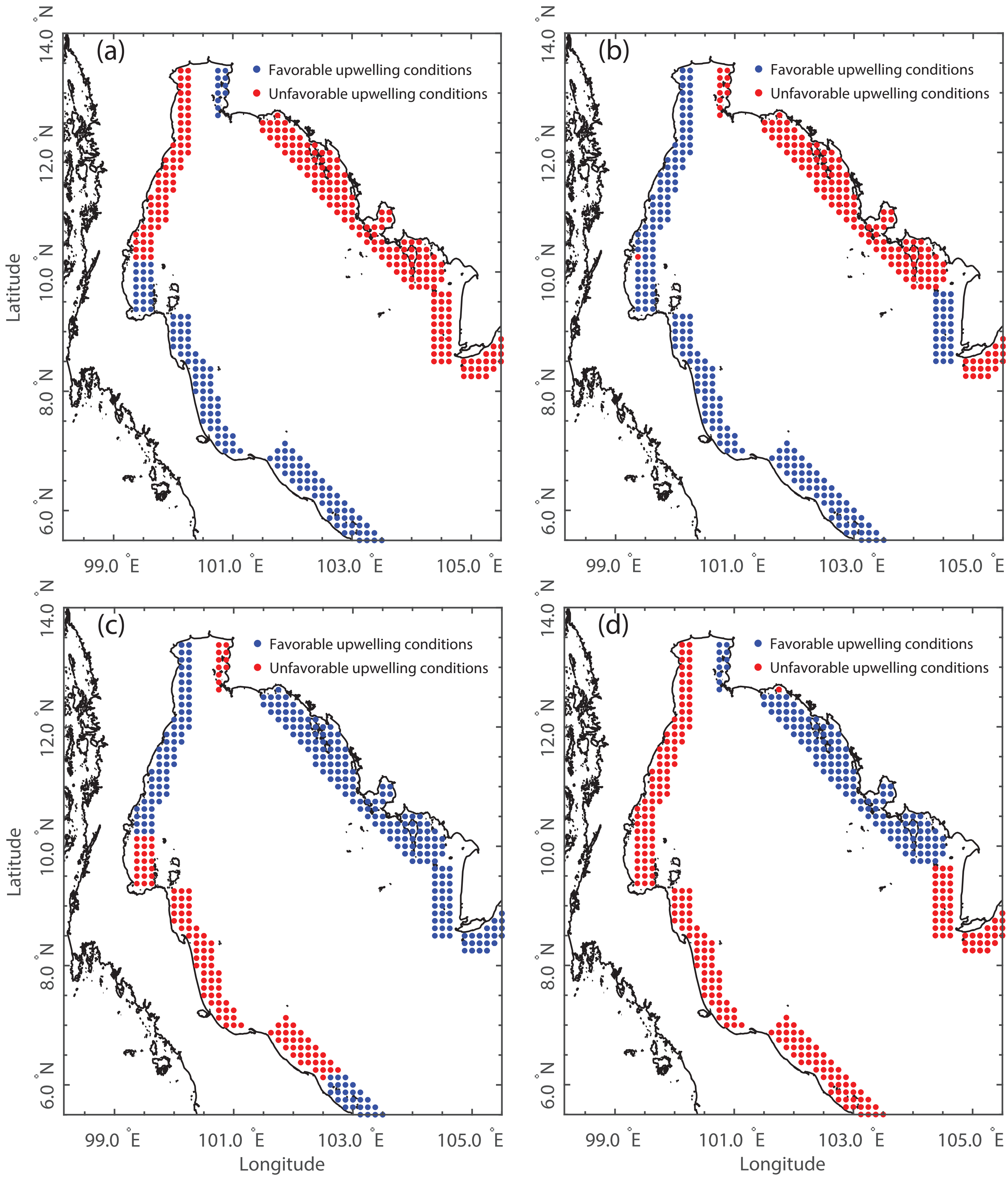

Fig. 4. Upwelling condition based on Ekman transport upwelling Index (UI_{ET}) in (a) January (Northeast monsoon), (b) March (1st inter-monsoon), (c) August (Southwest monsoon) and (d) October (2nd inter-monsoon). Blue and red dots denote favorable and unfavorable upwelling condition, respectively.

3.3. Sea Surface Temperature and UI_{SST}

Seasonal sea surface temperature (16 years monthly averaged) is shown in Fig. 5. In January, the cooler water (25.0–29.0 degree Celsius) was present for the whole Gulf (see Fig. 5(a)). In addition, the clear cooler front of 27.0–28.0 degree Celsius were found at west coast of the Upper Gulf and 27.0–28.0 degree Celsius at Lower Gulf (near Ca Mau Cape, Vietnam). Since northeast-

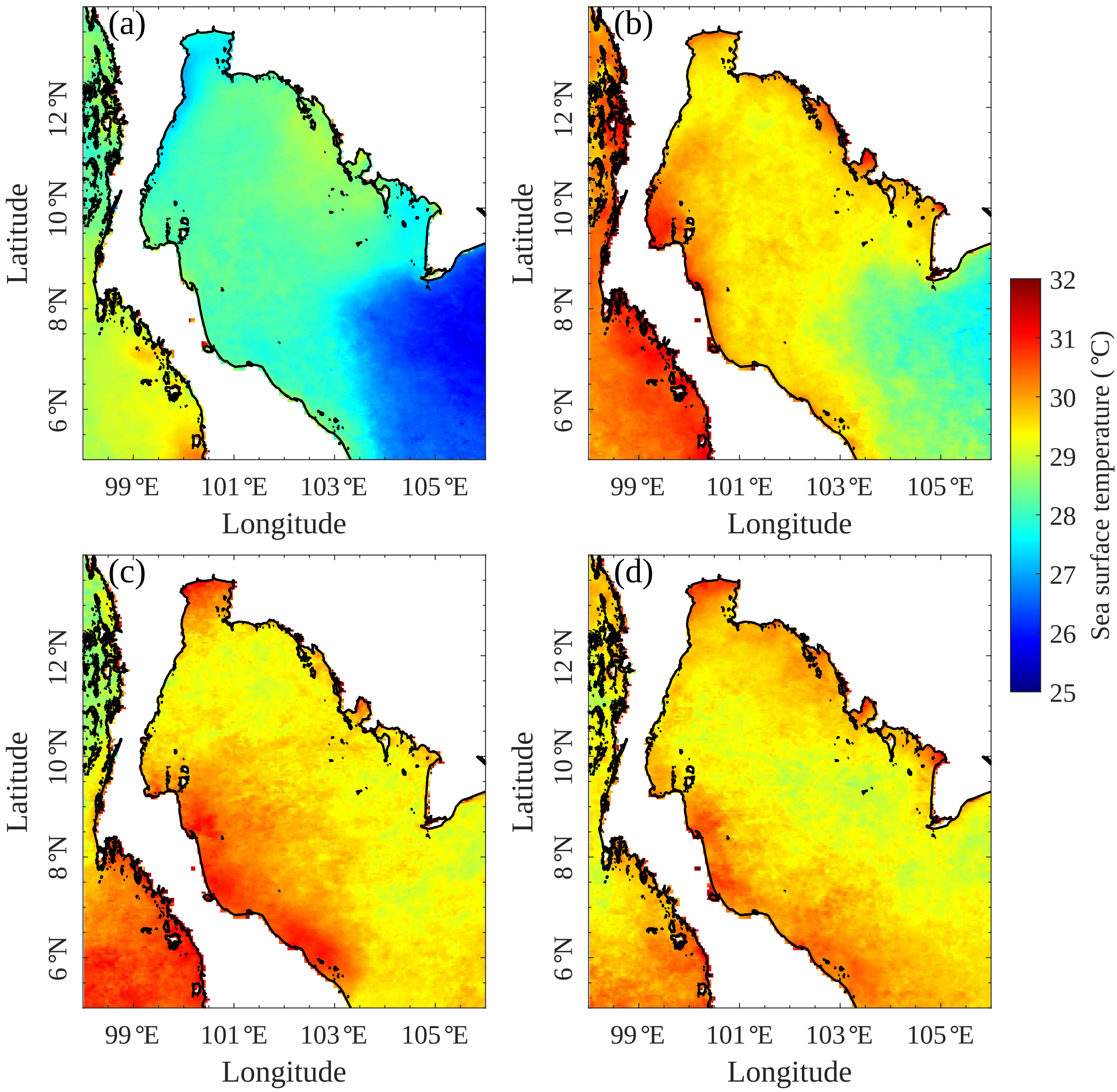

Fig. 5. Averaged sea surface temperature (degree Celsius) during year 2003–2018 in (a) January (Northeast monsoon), (b) March (1st inter-monsoon), (c) August (Southwest monsoon) and (d) October (2nd inter-monsoon).

erly wind dominates in the Upper Gulf, the surface flow was pushed to the west and left the Upper Gulf to the Central Gulf along the west coast. That is why cooler front along west coast of Upper Gulf and Central Gulf was observed during this period. In addition, the appearance of cooler water near the GoT's entrance was a result of the intrusion of the cooler SCS water mass due to strong northwestward Ekman transport (see section 3.2 and Fig. 3(a) for more detail explanation). These cooler signals (the temperature dropped to 27.0–29.0 degree Celsius) continued to exist near Ca Mau Cape during first inter-monsoon (see Fig. 4(b)). Conversely, in the Upper Gulf, the cooler water-front disappeared and instead warm water (29.0–32.0 degree Celsius) was developed, especially in the northern part of the Upper Gulf. Generally, the warm water initially occurred during first inter-monsoon and continued to develop for the whole GoT (the temperature around 29.5 degree Celsius). The warmer SST was formed mostly in the shallow area. Then, during southwest monsoon (see Fig. 5(c)), the warmer water in the Upper Gulf (temperature around 31.0–32.0 degree Celsius) dispersed southward towards the Central Gulf. It is similar to the one found near the west coast of the Lower Gulf. However, the temperature of water in the Central Gulf and Lower Gulf, especially near the east coast, remained the same. The temperature near the GoT's entrance was also warmer than the previous monsoon.

For the second inter-monsoon, the wide patch of cooler water of 28.5–29.5 degree Celsius was found at the center of the GoT and the east GoT to Ca Mau Cape. The spread of warmer water seaward found in the Upper Gulf and along the west coast of the Lower Gulf seemed to decrease. This pattern seemed to concentrate near the coastline. From Fig. 5, it is clearly seen that the SST in the GoT changed seasonally. During the northeast monsoon, the SST was cooler than other periods due to the net heat loss in the wintertime. Colder water from the SCS intruded into the GoT through the GoT's entrance between Kotabaru, Malaysia and Ca Mau Cape, Vietnam. During the first and second inter-monsoon and southwest monsoon, the warm SST existed almost for the whole gulf due to the net heat gain during summertime. However, the intrusion of colder water from the SCS still remain during the first inter-monsoon. This signal disappeared during southwest and second inter-monsoon. The characteristics of SST found in the GoT will be utilized to obtain the SST upwelling index later and will be discussed as follows.

Figures 6 and 7 depict sea surface temperature upwelling index (UI_{SST}) and sea surface temperature

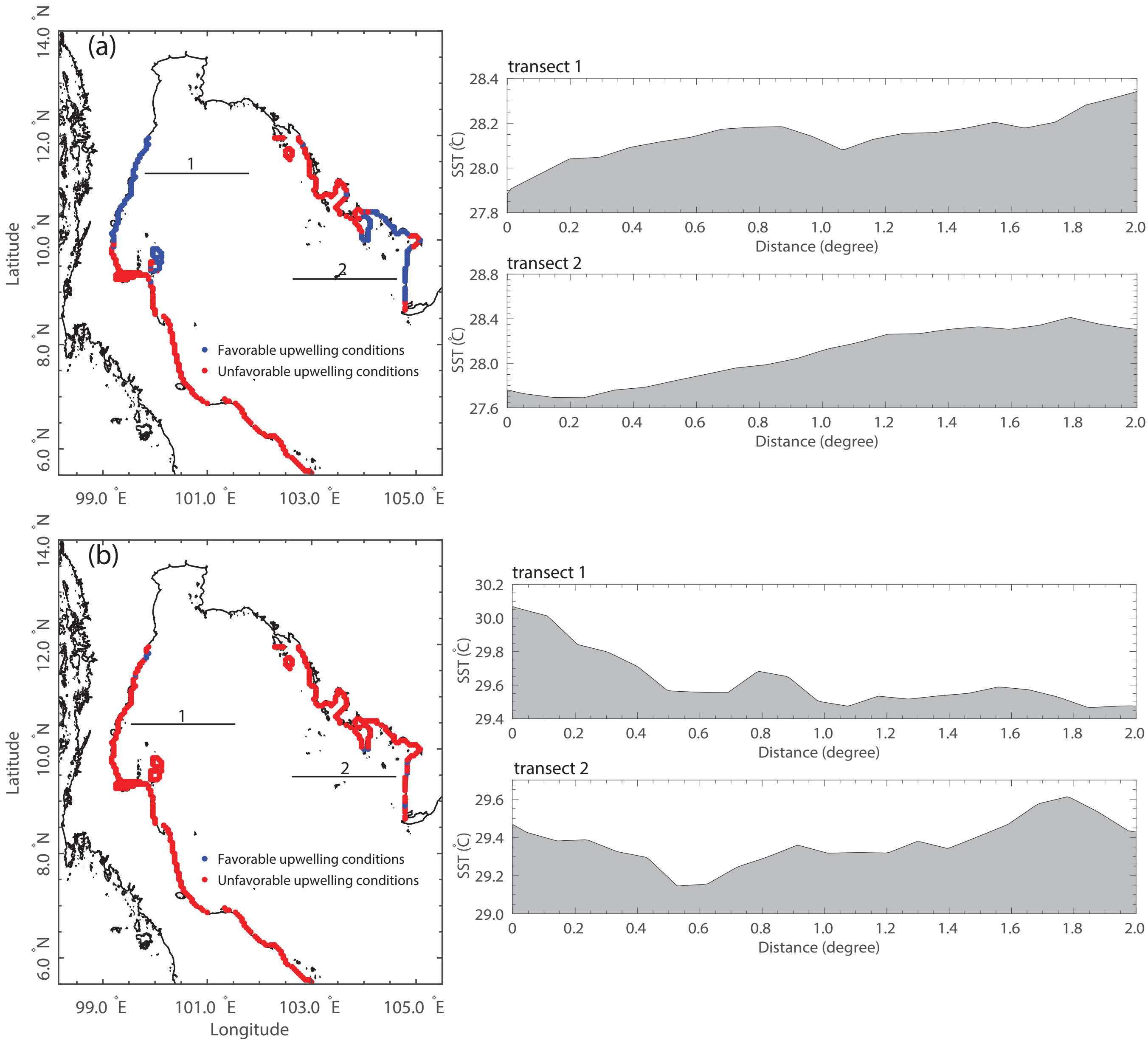

Fig. 6. Sea surface temperature upwelling index (UI_{SST}) (left) and temperature cross section profile (right) of line number 1 (upper) and line number 2 (bottom) extracted from shoreline to offshore in (a) January (Northeast monsoon) and (b) March (1st Inter-monsoon). Blue and red dots denote favorable and unfavorable upwelling condition, respectively.

DOI:10.4186/ej.2021.25.7.1

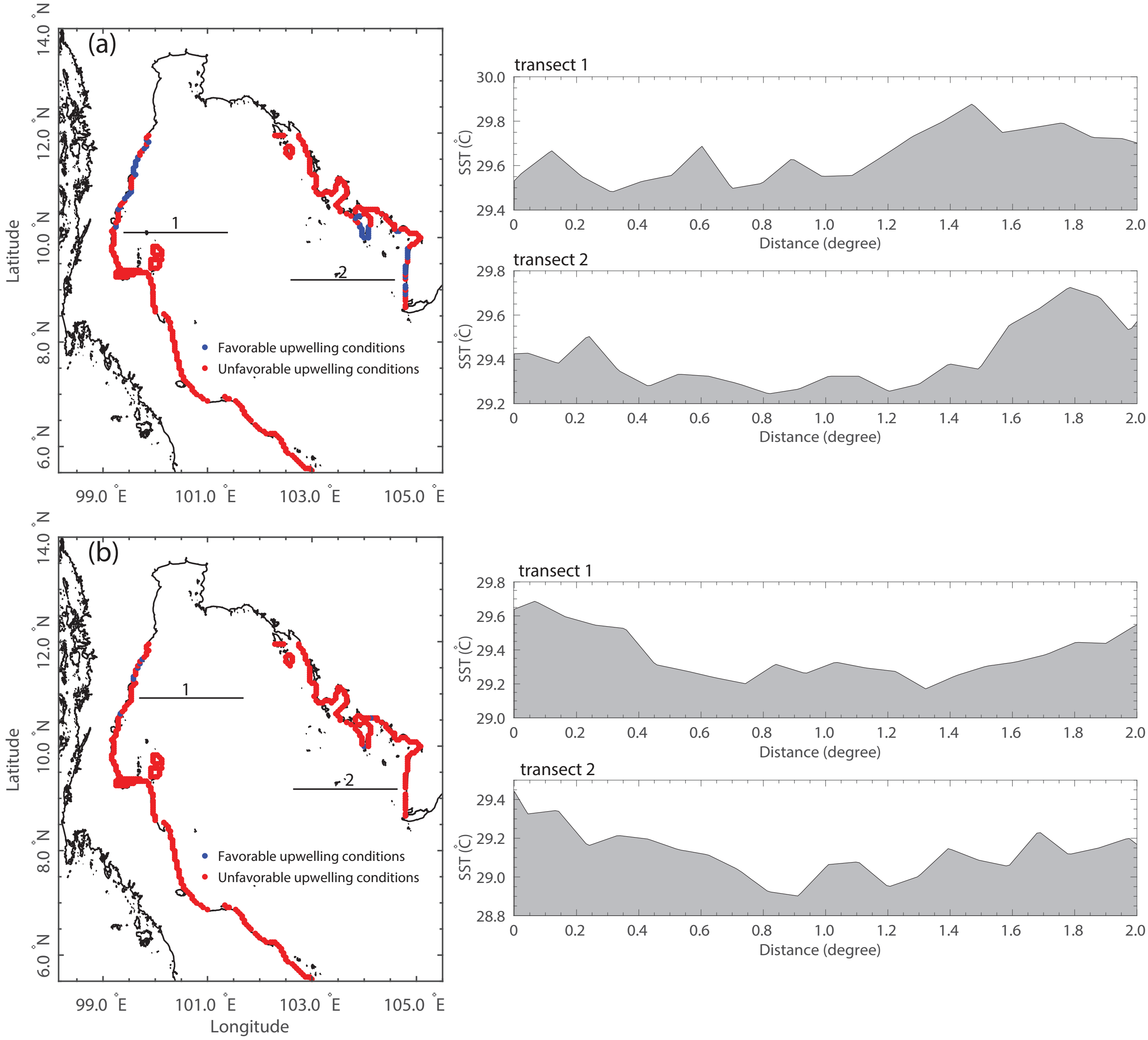

Fig. 7. Sea surface temperature upwelling index (UI_{SST}) (left) and temperature cross section profile (right) of line number 1 (upper) and line number 2 (bottom) extracted from shoreline to offshore in (a) August (Southwest monsoon) and (b) October (2^{nd} Inter-monsoon).

along 2 example line transects 1 and 2 (the distance is measured from shoreline toward offshore in degree longitude off west and east coast of the GoT, respectively) at 4 different periods. In general, the higher the temperature offshore means the favorable upwelling condition to be existed. Hence, the favorable upwelling conditions (blue color dots) estimated from sea surface temperature upwelling index as mentioned in section 2.2 appeared in January during northeast monsoon and in August during southwest monsoon. In January (see Fig. 6(a)), the favorable condition occurred along the west coast and around Samui Island with about 0.6 degree Celsius temperature difference, and along the south of east coast around Ca Mau Cape with approximately 0.8 degree Celsius temperature difference. In August (see Fig. 7(a)), the upwelling condition existed along the west coast with the temperature difference of 0.6 degree Celsius, and near the Ca Mau Cape with the temperature difference about 0.4 degree Celsius.

Based on the results shown above, it is apparent that upwelling conditions mostly occurred during northeast and southwest monsoons. And, they can be seen only in the northern part of the west gulf and the west coast of Ca Mau Cape. For the rest of the GoT, the unfavorable upwelling conditions were the most prominent. These unfavorable conditions still existed for the whole gulf during the first inter-monsoon (see Fig. 6(b)) and the second inter-monsoon (see Fig. 7(b)) as seen in the temperature difference along transects 1 and 2, which showed the higher coastal sea surface temperature than the oceanic sea surface temperature.

3.4. UI_{ET} and UI_{SST} Indices Relations in GoT

As mentioned in sections 3.2 and 3.3, sea surface temperature upwelling index (UI_{SST}) demonstrated the existence of seasonal patterns of upwelling during northeast monsoon and southwest monsoon along the northern part of the west coast of GoT and the western part of Ca Mau Cape. In addition, this signal also existed around Samui Island during northeast monsoon. When comparing with Ekman transport upwelling index (UI_{ET}), the area around Samui Island was in agreement during northeast monsoon. Meanwhile, during southwest monsoon, favorable upwelling condition found along the northern part of west coast of GoT and west coast of Ca Mau Cape were in agreement. From these results, there were several locations in the GoT with favorable upwelling condition as shown by UI_{SST} and UI_{ET} were in disagreement when compared between these two indices. There are a number of reasons to explain such discrepancy.

Firstly, coastal upwelling is an effect of Ekman transport, the current pushing the surface water offshore as a result of the steady and slowly varying alongshore wind stresses and the Earth's rotation. The current velocity is typically 0.05–0.10 m/s with the layer extending from surface to the depth about 100 m [37, 38, 39]. The Ekman transport upwelling estimation (wind-driven transport) is typically better used to investigate the upwelling condition in the ocean where the water depth is sufficiently deep [9, 26, 40] for the Ekman depth to be developed. Conversely, the GoT is generally a wide and moderately shallow basin with an average depth of 45 m and maximum depth of 80 m [13, 41]. Therefore, in the GoT it may be not deep enough for the Ekman depth to fully develop. Hence, the Ekman transport may not account for the whole Ekman depth. As a result, the transport of surface water will deviate to the right of wind direction less than 90 degree (in general, the Ekman transport is the transport of surface water 90 degree to the right of wind direction).

Secondly, since the GoT is shallow, the bottom friction will affect surface currents that are generated by monsoons wind. Therefore, the surface velocity may not veer 45 degree to the right of wind direction as theory suggests. This will ultimately affect the direction of transport of surface water due to wind as well.

Lastly, for UI_{SST}, sea surface temperature variation may be biased by several external factors including local-scale factors (e.g., river runoff which can alter sea surface temperature nearshore) and macro-scale factors (e.g., El Niño or La Niña events may also change coastal sea surface temperature that is not corresponding to coastal upwelling) [42].

3.5. Inter-annual and annual variability of UI_{ET} in the GoT

As described in [32, 42], UI_{ET} and UI_{SST} indices can be used to evaluate upwelling favorable condition in the coastal area, but UI_{SST} seems to more sensitive to the change in temperature caused by external forcings. Hence, in this section only the spatio-temporal signal of UI_{ET} presented in the GoT is discussed.

Unlike previous sections, 16-year of monthly UI_{ET} during 2003 to 2018 at the points along the West GoT and East GoT (red asterisks and red crosses shown in Fig. 1) together with monthly mean UI_{ET} were visualized using Hovmöller diagram as depicted in Figs. 8 and 9, respectively. From Fig. 8, favorable upwelling (positive value) and unfavorable upwelling (negative value) conditions over 16 years along the West GoT (Fig. 8(a)) and East GoT (Fig. 8(b)) coasts are clearly differentiated.

For the West GoT case, line transect covers area between latitude 5.25°N and 13.25°N. Stronger favorable upwelling signal seemed to occur at the southern most of Lower Gulf, especially during January to March, while less favorable upwelling signal appeared for both Upper and Lower Gulfs (see Fig. 8(a)). In the Central and Upper Gulfs, unfavorable upwelling signal was more pronounce than the Lower Gulf. Strongest unfavorable upwelling signal (more negative value) was found in 2009, while less unfavorable upwelling signal was found in 2013. In addition, these signals seemed to well relate to Multivariate ENSO Index (MEI). During the strong La Ninã condition or negative MEI, it was the condition that strong unfavorable upwelling signal occurred, while less La Ninã or El Ninõ conditions, less unfavorable upwelling signal was observed. Noted that, MEI signal is not presented here.

For the East GoT case, line transect covers area between latitude 8.50°N and 13.25°N. This line transect is shorter than West GoT case, starting from Ca Mau Cape to Upper Gulf. Strong unfavorable upwelling signals were observed in Upper Gulf and southern most of Central Gulf (see Fig. 8(b)). However, favorable upwelling signal also existed in the Central Gulf during the second half of the year, especially in the northern part.

Figure 8(c) presents inter-annual variability of meridional monthly averaged UI_{ET} during 2003 to 2018, where blue and red solid lines represent West GoT and East GoT transects, respectively. Favorable upwelling signal was dominant in West GoT transect than in East GoT transect and vice versa for unfavorable upwelling signal. These signals show periodicity both annually and inter-annually. Around January 2005, 2010,

DOI:10.4186/ej.2021.25.7.1

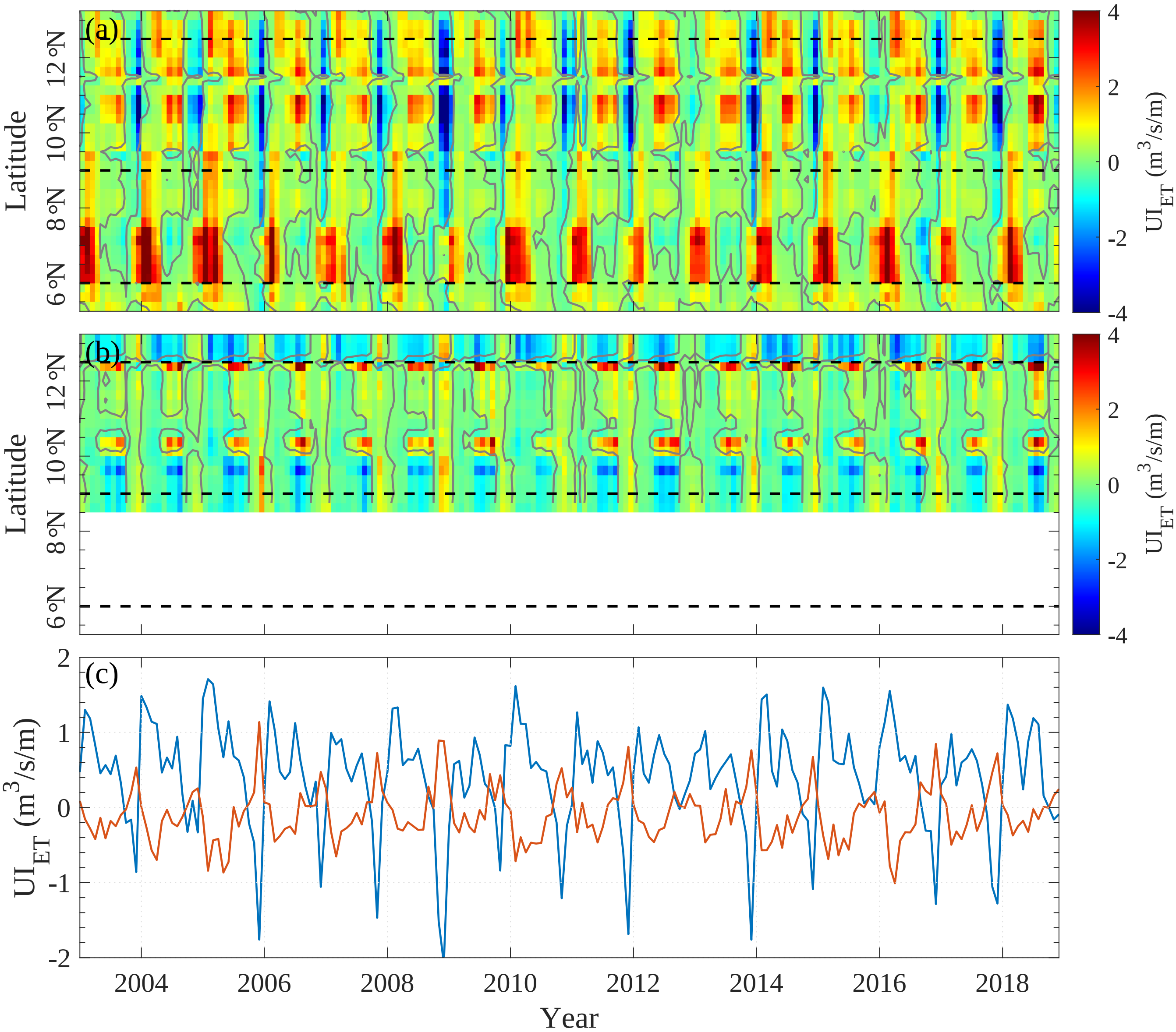

Fig. 8. (a) Inter-annual variability of monthly UI_{ET} during 2003 to 2018 along West GoT and (b) East GoT. Positive and negative UI_{ET} are separated by gray solid lines. The Upper Gulf, Central Gulf, and Lower Gulf are separated by dashed lines. (c) Inter-annual variability of meridional monthly averaged UI_{ET}, where blue and red solid lines are for West GoT and East GoT, respectively.

2014, 2015, and 2016 showed the peak of favorable upwelling condition for West GoT, while December 2005, 2009, 2012, and 2014 showed the peak of unfavorable upwelling condition. As mentioned above, for West GoT the signal of UI_{ET} was mostly above zero for the first third-fourth of the year. Unlike West GoT transect, UI_{ET} of East GoT seemed to have unfavorable upwelling condition dominated. However, it can be seen that peak of favorable upwelling condition was observed in December of all year round. In general, upwelling and downwelling conditions based on Ekman transport theory in the GoT was occurred seasonally depending on geographic location, shape of coastline (regular or irregular), and monsoon wind. In some areas, favorable upwelling condition existed during summer and disappeared during winter monsoon. Unlike the major eastern upwelling system (e.g., Iberian Peninsula [26] and Canary upwelling system [32]), upwelling condition was observed all year round. Furthermore, coastlines for all major upwelling systems seemed to have a regular shape (i.e., straight coastline), while local upwelling system (e.g., Eastern Malaysian Peninsula [11] and Vietnam coast [3]), changed seasonally. Hence, the seasonal pattern of UI_{ET} in the GoT will be investigated by applying monthly averaged for all 16 years (2003–2018) UI_{ET} data.

Figure 9 shows 16-year averaged annual variability of UI_{ET} during 2003 to 2018 for the West GoT (Fig.

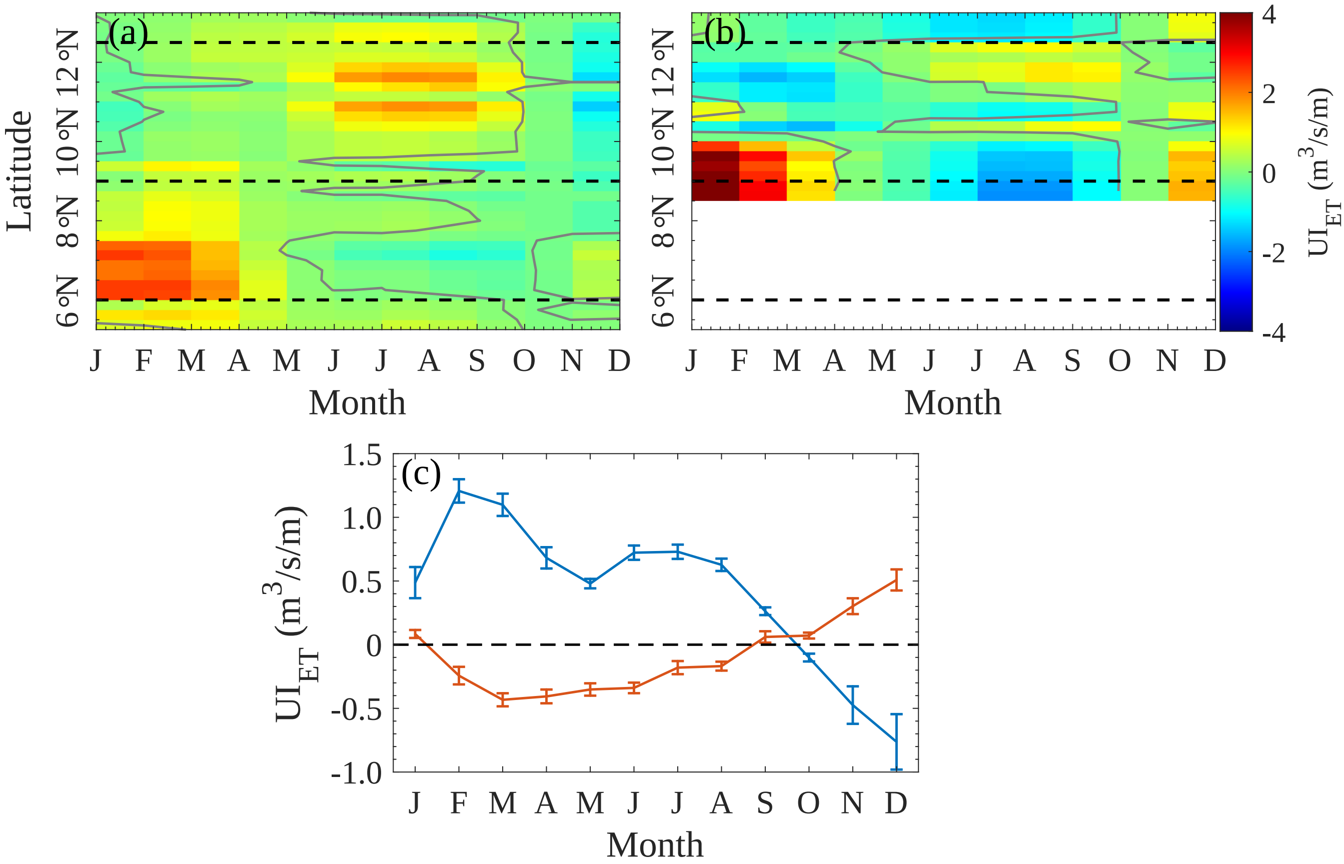

Fig. 9. 16-year averaged annual variability of UI_{ET} during 2003 to 2018 along (a) West GoT and (b) East GoT. Gray solid line denotes zero UI_{ET}. The Upper Gulf, Central Gulf, and Lower Gulf are separated by dashed lines. (c) Annual variation of meridional monthly averaged UI_{ET}, where blue and red solid lines are for West GoT and East GoT, respectively.

9(a)) and East GoT (Fig. 9(b)) transects. In this figure, seasonal and spatial variation of UI_{ET} in GoT is easily distinguishable. As seen in Fig. 9(a), the favorable upwelling condition appeared in Central Gulf and Upper Gulf during February to October and the rest was unfavorable upwelling condition. These signals were related to monsoon winds that prevailed in Southeast Asian region, where northeast and southwest monsoon winds blew during winter and summer seasons, respectively. At the lower end of Central Gulf, favorable upwelling condition was pronounced from January to September (about 8 months).

In Thailand, the Department of Fisheries closes the area between latitude 9.00°N and 12.00°N during mid-February to mid-May to allow short mackerel to spawn and another 1 month to allow fish larvae to migrate up north and reach the juvenile stage in the Upper Gulf. This may relate to favorable upwelling condition that existed during February to October as mentioned above. In addition, located at the lower end of Central Gulf is Sumui Island, where high chlorophyll_a concentration (a proxy of high productivity) exist [18] and it is an area rich of biodiversity of marine resources [20]. In the Lower Gulf, strong favorable upwelling condition, especially the southern part, dominated between January and July. Short period (July to November) was for less unfavorable upwelling condition to dominate.

For East GoT UI_{ET} transect (Fig. 9(b)), it was found that unfavorable upwelling condition in Upper Gulf dominated for all most the year except during northeast monsoon between October to February. In Central Gulf, strong favorable upwelling condition existed near the southern part between October to April during the northeast monsoon. As previously mentioned, upwelling condition in the same latitude for both transects was in opposite for the whole period.

Annual variation of meridional monthly averaged UI_{ET} along West GoT (blue solid line) and East GoT (red solid line) transects were plotted and showed in Fig. 9(c). This figure was obtained by meridionally averaged monthly data as seen in Figs. 9(a) and 9(b). Error bars for each month were estimated form standard deviation of UI_{ET} divided by squared root of number of year ($\sigma(UI_{ET})/\sqrt{N}$), where N in this case is 16 years. For West GoT transect, there were two peaks of favorable upwelling condition (February and July), while peak of unfavorable upwelling condition was in December. Favorable upwelling condition was observed almost for the whole year, except between October and December, when unfavorable upwelling condition were presented. This might be explained by northeast monsoon pushed surface water toward the West GoT's coast (see Fig. 2(a)) causing downwelling to be occurred along the west coast.

For East GoT UI_{ET} transect, peak of favorable upwelling condition was found in December (see Fig. 9(c)) because northeast monsoon wind pushed water toward west coast (see Fig. 2(c)), causing underneath subsurface water to compensate offshore transport water above. On the other hands, unfavorable upwelling condition was found between February and August with March as a peak of unfavorable upwelling condition. It can be noticed that southwest monsoon wind pushed surface from west coast toward east coast causing downwelling to be occurred in east coast, which were in agreement with previous studies (e.g., [14, 15, 16]). The signals found in East GoT transect was opposite to what have been observed in West GoT transect.

4. Conclusion

The possibly coastal upwelling in the GoT was investigated through the analysis of Ekman transport upwelling index (UI_{ET}) estimation based on wind velocity components, and sea surface temperature upwelling index (UI_{SST}) estimation. The monthly mean wind velocity data showed wind patterns which were northeasterly winds during northeast monsoon and southwesterly winds during southwest monsoon. During northeast monsoon, Ekman transport caused northwestward movement of SCS water into the GoT. Water in the GoT was transported out as a result of southeastward Ekman transport during southwest monsoon. These 2 signals in both monsoons impacted seasonal variation of monthly mean sea level found in the GoT, which is high during northeast monsoon and low during southwest monsoon. According to the estimations of Ekman transport upwelling and sea surface temperature upwelling, they expressed favorable upwelling conditions along the west coast and Ca Mau Cape during southwest monsoon. Spatially favorable upwelling condition found in the GoT based on Ekman transport estimation was variable due to spatial variation of seasonal wind pattern. Disagreement between UI_{SST} and UI_{ET} indices found from this study may get affected by the shallowness of the GoT and bottom friction (invalidity of using Ekman transport theory).

Inter-annual variability of meridionally averaged UI_{ET} estimated along the east coast and west coast of GoT depicted oppositely periodicity of favorable and unfavorable upwelling conditions. The inter-annual variability of UI_{ET} seemed to well associate with Multivariate ENSO Index. Strong unfavorable upwelling signal occurred during strong La Ninã condition, while less unfavorable upwelling condition was observed during weak La Ninã or El Ninõ conditions. From Annual variability of UI_{ET}, along West GoT's coast, where favorable upwelling condition was dominant, especially during southwest monsoon, except October to December (during northeast monsoon). Along the East GoT's coast, unfavorable upwelling condition was the most prominent, but favorable upwelling condition was found during northeast monsoon (October to January).

The result from this study can be used for fishery management in the GoT. However, in order to complete the knowledge about coastal upwelling in the GoT and to confirm our findings, other research studies are required.

Acknowledgements

The authors would like to express their gratitude to the scholarship from Graduate School, Chulalongkorn University to commemorate the 72nd anniversary of his Majesty King Bhumibhol Adulyadej. This study is partially supported by Thailand Science Research and Innovation (No. SRI5830703).

We are very grateful to valuable comments and suggestions from two anonymous reviewers that help to enhance the quality of the manuscript and Dr. Chawalit Charoenpong for improving the use of English in the manuscript.

References

[1] M. Tomczak and J. S. Godfrey, *Regional Oceanography: An Introduction*. Pergamon, 1994, ch. Ekman layer transports, Ekman pumping and the Sverdrup balance, pp. 39–51.

[2] M. Messié, J. Ledesma, D. D. Kolber, R. P. Michisaki, D. G. Foley, and F. P. Chavez, "Potential new production estimates in four eastern boundary upwelling ecosystems," *Progress in Oceanography*, vol. 83, no. 1, pp. 151–158, 2009.

[3] J. Dippner, K. Nguyen, H. Hein, T. Ohde, and N. Loick, "Monsoon–induced upwelling off the Vietnamese coast," *Ocean Dynamics*, vol. 57, pp. 46–62, 2007.

[4] A. Lehmann and K. Myrberg, "Upwelling in the Baltic Sea – A review," *Journal of Marine Systems*, vol. 74, pp. S3–S12, 2008.

[5] H. Hein, B. Hein, T. Pohlmann, and B. H. Long, "Inter-annual variability of upwelling off the

South–Vietnamese coast and its relation to nutrient dynamics," *Global and Planetary Change*, vol. 110, pp. 170–182, 2013.

[6] A. Bakun, "Coastal upwelling indices, West coast of North America, 1946-71." NOAA, Tech. Rep., 1973.

[7] ——, "Daily and weekly upwelling indices, West coast of North America, 1967-73." NOAA, Tech. Rep., 1975.

[8] J. Kämpf and P. Chapman, *Upwelling Systems of the World*. Springer, Cham, 2016, ch. The functioning of coastal upwelling systems, pp. 31–65.

[9] P. C. Pardo, X. Padin, M. Gilcoto, L. Farina-Busto, and F. Perez, "Evolution of upwelling systems coupled to the long–term variability in sea surface temperature and Ekman transport," *Climate Research*, vol. 48, pp. 231–246, 2011.

[10] T. E. Cropper, E. Hanna, and G. R. Bigg, "Spatial and temporal seasonal trends in coastal upwelling off Northwest Africa, 1981–2012," *Deep Sea Research Part I: Oceanographic Research Papers*, vol. 86, pp. 94–111, 2014.

[11] P. H. Kok, M. F. Mohd Akhir, F. Tangang, and M. L. Husain, "Spatiotemporal trends in the southwest monsoon wind–driven upwelling in the southwestern part of the South China Sea," *PLOS ONE*, vol. 12, no. 2, pp. 1–22, 2017.

[12] W. Burnett, G. Wattayakorn, M. Taniguchi, H. Dulaiova, P. Sojisuporn, S. Rungsupa, and T. Ishitobi, "Groundwater–derived nutrient inputs to the Upper Gulf of Thailand," *Continental Shelf Research*, vol. 27, pp. 176–190, 2007.

[13] S. Liu, H. Zhang, A. Zhu, K. Wang, M.-T. Chen, S. Khokiattiwong, N. Kornkanitnan, and X. Shi, "Distribution of rare earth elements in surface sediments of the western Gulf of Thailand: Constraints from sedimentology and mineralogy," *Quaternary International*, vol. 527, pp. 52–63, 2019.

[14] D. Cushing, "Upwelling and the production of fish," in *Advances in Marine Biology*, F. S. Russell and M. Yonge, Eds. Academic Press, 1971, vol. 9, pp. 255–334.

[15] M. K. Robinson, *NAGA Report Volume 3, Part 1*. Scripps Institution of Oceanography, 1974, ch. The physical oceanography of the Gulf of Thailand, Naga Expedition, pp. 5–110.

[16] P. Sojisuporn, A. Morimoto, and T. Yanagi, "Seasonal variation of sea surface current in the Gulf of Thailand," *Coastal Marine Science*, vol. 34, pp. 91–102, 2010.

[17] T. Yanagi and T. Takao, "Seasonal variation of three-dimensional circulation in the Gulf of Thailand," *La mer*, vol. 36, pp. 43–55, 1998.

[18] P. Singhruck, "Circulation features in the Gulf of Thailand inferred from SeaWiFS data," in *the 22nd Asian Conference on Remote Sensing*, National University of Singapore, 2001, p. 4.

[19] R. Green, "Community perceptions of environmental and social change and tourism development on the island of Koh Samui, Thailand," *Journal of Environmental Psychology*, vol. 25, no. 1, pp. 37–56, 2005.

[20] V. Vilasri, T. Onodera, T. Kawai, H. Imamura, and C. Kawagoe, "Survey for coastal fishes in near shore habitat of Samui Island, Thailand," *The Thailand Natural History Museum Journal*, vol. 12, no. 1, pp. 29–34, 2018.

[21] M. Ahmed, P. Boonchuwongs, W. Dechboon, and D. Squires, "Overfishing in the Gulf of Thailand: Policy challenges and bioeconomic analysis," *Environment and Development Economics*, vol. 12, pp. 145–172, 2007.

[22] S. Ingthamjitr and B. Sricharoendham, "Current status of fish stock enhancement in Thailand," in *the Symposium on Strategy for Fisheries Resources Enhancement in the Southeast Asian Region*, Southeast Asian Fisheries Development Center, Training Department, 2016, pp. 144–148.

[23] SEAFDEC, "Report of the experts group meeting on stock status and geographical distribution of Anchovy, Indo-Pacific Mackerel and Blue Swimming Crab (AIB) species in the Gulf of Thailand," Souhteast Asian Fisheries Development Center, Bangkok, Thailand, 22-23 September 2016, Tech. Rep., 2017.

[24] S. Kongseng, R. Phoonsawat, and A. Swatdipong, "Individual assignment and mixed-stock analysis of short mackerel (*Rastrelliger brachysoma*) in the Inner and Eastern Gulf of Thailand: Contrast migratory behavior among the fishery stocks," *Fisheries Research*, vol. 221, p. 105372, 2020.

[25] D. P. Dee, S. M. Uppala, A. J. Simmons, P. Berrisford, P. Poli, S. Kobayashi, U. Andrae, M. A. Balmaseda, G. Balsamo, P. Bauer, P. Bechtold, A. C. M. Beljaars, L. van de Berg, J. Bidlot, N. Bormann, C. Delsol, R. Dragani, M. Fuentes, A. J. Geer, L. Haimberger, S. B. Healy, H. Hersbach, E. V. Hólm, L. Isaksen, P. Kållberg, M. Köhler, M. Matricardi, A. P. McNally, B. M. Monge-Sanz, J.-J. Morcrette, B.-K. Park, C. Peubey, P. de Rosnay, C. Tavolato, J.-N. Thépaut, and F. Vitart, "The ERA-Interim reanalysis: configuration and performance of the data assimilation system," *Quarterly Journal of the Royal Meteorological Society*, vol. 137, no. 656, pp. 553–597, 2011.

[26] I. Alvarez, M. Gomez-Gesteira, M. deCastro, M. Lorenzo, A. Crespo, and J. Dias, "Comparative

analysis of upwelling influence between the western and northern coast of the Iberian Peninsula," *Continental Shelf Research*, vol. 31, no. 5, pp. 388–399, 2011.

[27] F. Santos, M. Gomez-Gesteira, M. deCastro, and I. Alvarez, "Differences in coastal and oceanic SST trends due to the strengthening of coastal upwelling along the Benguela current system," *Continental Shelf Research*, vol. 34, pp. 79–86, 2012.

[28] W. Yin and D. Huang, "Short–Term variations in the surface upwelling off Northeastern Taiwan observed via satellite data," *Journal of Geophysical Research: Oceans*, vol. 124, no. 2, pp. 939–954, 2019.

[29] Y. Yu, Y. Wang, L. Cao, R. Tang, and F. Chai, "The ocean–atmosphere interaction over a summer upwelling system in the south china sea," *Journal of Marine Systems*, vol. 208, p. 103360, 2020.

[30] J. Vazquez-Cuervo, B. Dewitte, T. M. Chin, E. M. Armstrong, S. Purca, and E. Alburqueque, "An analysis of sst gradients off the Peruvian coast: The impact of going to higher resolution," *Remote Sensing of Environment*, vol. 131, pp. 76 – 84, 2013.

[31] T. M. Chin, J. Vazquez-Cuervo, and E. M. Armstrong, "A multi-scale high-resolution analysis of global sea surface temperature," *Remote Sensing of Environment*, vol. 200, pp. 154 – 169, 2017.

[32] M. Gómez-Gesteira, M. De Castro, I. Álvarez, M. N. Lorenzo, J. L. G. Gesteira, and A. J. C. Crespo, "Spatio-temporal upwelling trends along the Canary upwelling system (1967–2006)," *Annals of the New York Academy of Sciences*, vol. 1146, no. 1, pp. 320–337, 2008.

[33] A. Benazzouz, S. Mordane, A. Orbi, M. Chagdali, K. Hilmi, A. Atillah, J. Lluís Pelegrí, and D. Hervé, "An improved coastal upwelling index from sea surface temperature using satellite-based approach – the case of the canary current upwelling system," *Continental Shelf Research*, vol. 81, pp. 38–54, 2014.

[34] P.-T. Shaw and S.-Y. Chao, "Surface circulation in the South China Sea," *Deep Sea Research Part I: Oceanographic Research Papers*, vol. 41, no. 11, pp. 1663–1683, 1994.

[35] S. Saramul and T. Ezer, "Spatial variations of sea level along the coast of Thailand: Impacts of extreme land subsidence, earthquakes and the seasonal monsoon," *Global and Planetary Change*, vol. 122, pp. 70–81, 2014.

[36] S. Saramul, "Seasonal monsoon variations in surface currents in the Gulf of Thailand revealed by high frequency radar," *Engineering Journal*, vol. 21, no. 4, pp. 25–37, 2017.

[37] T. K. Chereskin and J. F. Price, "Upper ocean structure: Ekman transport and pumping," in *Encyclopedia of Ocean Sciences*, 3rd ed., J. K. Cochran, H. J. Bokuniewicz, and P. L. Yager, Eds. Oxford: Academic Press, 2019, pp. 80–85.

[38] M. H. Pickett and J. D. Paduan, "Ekman transport and pumping in the California Current based on the U.S. Navy's high–resolution atmospheric model (COAMPS)," *Journal of Geophysical Research: Oceans*, vol. 108, no. C10, 2003.

[39] I. Alvarez, M. Gomez-Gesteira, M. deCastro, and E. Novoa, "Ekman transport along the Galician Coast (NW, Spain) calculated from QuikSCAT winds," *Journal of Marine Systems*, vol. 72, no. 1, pp. 101–115, 2008.

[40] M. Gomez-Gesteira, C. Moreira, I. Alvarez, and M. deCastro, "Ekman transport along the Galician coast (northwest Spain) calculated from forecasted winds," *Journal of Geophysical Research: Oceans*, vol. 111, no. C10, 2006.

[41] S. Tomkratoke, S. Sirisup, V. Udomchoke, and J. Kanasut, "Influence of resonance on tide and storm surge in the Gulf of Thailand," *Continental Shelf Research*, vol. 109, pp. 112–126, 2015.

[42] M. Gómez-Gesteira, M. deCastro, I. Alvarez, and J. L. Gómez-Gesteira, "Coastal sea surface temperature warming trend along the continental part of the atlantic arc (1985–2005)," *Journal of Geophysical Research: Oceans*, vol. 113, no. C4, 2008.

[43] K. E. Trenberth, W. G. Large, and J. G. Olson, "The mean annual cycle in global ocean wind stress," *Journal of Physical Oceanography*, vol. 20, no. 11, pp. 1742 – 1760, 1990.

Pacharamon Sripoonpan, photo and biography not available at the time of publication.

Suriyan Saramul, photo and biography not available at the time of publication.